The *Caenorhabditis elegans* Patched domain protein PTR-4 is required for proper organization of the precuticular apical extracellular matrix

Jennifer D. Cohen,[1,†] Carla E. Cadena del Castillo,[2,†] Nicholas D. Serra,[1,†] Andres Kaech,[3] Anne Spang,[2] and Meera V. Sundaram [ID] [1,*]

[1]Department of Genetics, University of Pennsylvania Perelman School of Medicine, Philadelphia, Pennsylvania 19104, USA
[2]Biozentrum, University of Basel, 4001 Basel, Switzerland
[3]Center for Microscopy and Image Analysis, University of Zürich, 8006 Zürich, Switzerland
[†]These authors contributed equally to this study.

*Corresponding author: Department of Genetics, University of Pennsylvania Perelman School of Medicine, Philadelphia, PA, USA.
Email: sundaram@pennmedicine.upenn.edu

Abstract

The Patched-related superfamily of transmembrane proteins can transport lipids or other hydrophobic molecules across cell membranes. While the Hedgehog receptor Patched has been intensively studied, much less is known about the biological roles of other Patched-related family members. *Caenorhabditis elegans* has a large number of Patched-related proteins, despite lacking a canonical Hedgehog pathway. Here, we show that PTR-4 promotes the assembly of the precuticle apical extracellular matrix, a transient and molecularly distinct matrix that precedes and patterns the later collagenous cuticle or exoskeleton. *ptr-4* mutants share many phenotypes with precuticle mutants, including defects in eggshell dissolution, tube shaping, alae (cuticle ridge) structure, molting, and cuticle barrier function. PTR-4 localizes to the apical side of a subset of outward-facing epithelia, in a cyclical manner that peaks when precuticle matrix is present. Finally, PTR-4 is required to limit the accumulation of the lipocalin LPR-3 and to properly localize the Zona Pellucida domain protein LET-653 within the precuticle. We propose that PTR-4 transports lipids or other hydrophobic components that help to organize the precuticle and that the cuticle and molting defects seen in *ptr-4* mutants result at least in part from earlier disorganization of the precuticle.

Keywords: *C. elegans*; patched-related; extracellular matrix; cuticle; PTR-4

Introduction

Patched (PTCH) and other Patched-related (PTR) or Patched domain (PTCHD) proteins are members of a large, evolutionarily conserved family of small molecule and lipid transporters (Zhong et al. 2014). All are multipass transmembrane proteins with a predicted hydrophobic cleft to transport hydrophobic cargo or bind ligands, and all share structural homology with archaeal and bacterial resistance-nodulation division (RND) transporters (Nikaido 2018). Many organisms express multiple PTR proteins, which share a sterol sensing domain (SSD) and similar overall structure with classical PTCH proteins but show considerable sequence divergence (Kuwabara and Labouesse 2002). While PTCH has been studied extensively for its role in canonical Hedgehog (Hh) signaling (Zhong et al. 2014), much less is known about the roles of most other PTR proteins.

PTCH and several other broadly conserved PTR/PTCHD proteins transport cholesterol or lipid-modified proteins across cellular membranes. Although many details remain debated, recent evidence suggests that, in the absence of Hh signaling, PTCH transports cholesterol across the plasma membrane to locally inhibit the G-protein coupled receptor Smoothened (SMO). When Hh, a cholesterol-modified lipoprotein, binds the PTCH extracellular domain, it blocks cholesterol transport, allowing cholesterol to activate SMO signaling (Zhang et al. 2018; Hu and Song 2019; Petrov et al. 2020). Another PTCHD protein, Dispatched, exports Hh from cells (Hall et al. 2019). Yet another related protein, Npc1, exports cholesterol from lysosomes; mutations in *Npc1* lead to massive, cholesterol-filled lysosomes and severe cellular dysfunction (Nikaido 2018; Cologna and Rosenhouse-Dantsker 2019; Melly and Purdy 2019; Pfeffer 2019). In addition to PTCH, Dispatched, and Npc1, mammals express four different PTCHDs whose molecular functions are unknown, but which have intriguing possible links to disease. While they may not play a role in Hh signaling, at least PTCHD2 has been linked to the maintenance of cholesterol homeostasis (Zikova et al. 2009; Konířová et al. 2017). Loss of and mutations in PTCHD1 are associated with autism spectrum disorders (Chaudhry et al. 2015; Torrico et al. 2015; Ung et al. 2018). PTCHD4 appears to negatively regulate Hh signaling in cancer (Chung et al. 2014), while the function of the nonessential PTCHD3 remains elusive.

The roundworm *Caenorhabditis elegans* contains multiple PTCH, Dispatched, and Npc1-like proteins and more than 20 other PTR/PTCHD proteins, along with many unusual Hh-like proteins, but it lacks SMO and other members of the canonical Hh signaling pathway (Zugasti *et al.* 2005; Bürglin and Kuwabara 2006; Hao *et al.* 2006b; Bürglin 2008). We showed recently that the PTCH protein PTC-3 has cholesterol transport activity (Cadena del Castillo *et al.* 2019), while several other PTR proteins were suggested to transport Hh-like proteins (Chiyoda *et al.* 2021), act as PTCH-like receptors through unknown downstream signaling pathways (Templeman *et al.* 2020), or to play other roles in apically directed trafficking or endocytosis (Michaux *et al.* 2000; Perens and Shaham 2005). Nevertheless, the functions of most PTR proteins remain unknown, and it is not clear why *C. elegans* has so many PTR proteins compared to other organisms.

Previous studies showed that RNAi-mediated knockdown of many *C. elegans ptr* genes led to defects in cuticular structure and molting (Zugasti *et al.* 2005; Hao *et al.* 2006a), suggesting a potential role for PTR proteins in trafficking or export of components of the apical extracellular matrix (aECM). *Caenorhabditis elegans* has multiple distinct types of aECM, including a chitinous eggshell and a collagenous cuticle that must be disassembled and rebuilt during each of four larval molts (Page and Johnstone 2007; Stein and Golden 2018; Cohen and Sundaram 2020). Prior to the generation of each new cuticle, a molecularly distinct aECM, termed the sheath or precuticle, coats external epithelia (Priess and Hirsh 1986; Vuong-Brender *et al.* 2017; Cohen and Sundaram 2020; Cohen *et al.* 2020b). Mutants that disrupt the precuticle often have defects in cuticle organization and/or molting (Cohen and Sundaram 2020). We therefore wondered if PTR proteins might play a role in precuticle assembly.

Here, we report that one *ptr* gene, *ptr-4*, is required for precuticle aECM assembly. The precuticle is a transient aECM that contains multiple proteins of the Zona Pellucida (ZP) domain, extracellular leucine-rich repeat only (eLRRon), and lipocalin (putative lipid transporter) families (Mancuso *et al.* 2012; Kelley *et al.* 2015; Gill *et al.* 2016; Forman-Rubinsky *et al.* 2017; Vuong-Brender *et al.* 2017; Katz *et al.* 2018; Cohen *et al.* 2019; *et al.* 2020b). It is present in the developing embryo and prior to each larval molt, and it shapes multiple epithelial tissues and helps pattern the subsequent collagenous cuticle (Cohen and Sundaram 2020). We show that *ptr-4* mutants share many phenotypes with precuticle mutants, including defects in eggshell dissolution, tube shaping, alae (cuticle ridge) structure, and cuticle barrier function. PTR-4 localizes to apical surfaces of outward-facing epithelia during periods of precuticle assembly and remodeling, and in addition to affecting the pattern of several cuticle collagens, PTR-4 is required to restrict the accumulation of the lipocalin LPR-3 and to properly localize the ZP domain protein LET-653 within the precuticle aECM. Together, these data suggest a role for PTR-4 in the transport of precuticle aECM components.

Materials and methods
Worm strains, alleles, and transgenes
All strains were derived from Bristol N2 and were grown at 20°C under standard conditions (Brenner 1974). *ptr-4(cs273)* mutant embryos were obtained from mothers rescued with a *ptr-4(+)* transgene, *csEx888*. This transgene was generated by coinjecting fosmid WRM069dE04 at 15 ng/μl along with pIM175 (*unc-119::gfp*) at 30 ng/μl and SK+ at 100 ng/μl. The *ptr-4pro*::NLS-GFP transcriptional reporters *csEx943*, *csEx944*, and *csEx945* were generated by coinjecting plasmid pNDS1 at 30 ng/μl along with pRF4

[*rol-6(su1006)*] at 90 ng/μl. pNDS1 was generated by PCR amplifying 1.6 kb of *ptr-4* upstream sequence from template WRM069dE04 with primers oMS224 (TTTTTCCTGCAGCTCATA ACTCC) and oMS228 (GATCATGAGCTCGGTTAGGTCT GAACCCAACTGC), and cloning it as a PstI-SacI fragment into vector pPD121.83 (Addgene). See Supplementary Table S1 for a complete list of strains and alleles used.

ptr-4 mutant isolation and allele identification
The *ptr-4(cs264[PTR-4::SfGFP])*, *ptr-4(cs285 [PTR-4::mCherry])*, *ptr-4(cs273)*, and *ptr-4(cs279)* alleles were created in an N2 background by CRISPR-Cas9. *ptr-4(cs264[PTR-4::SfGFP])* and *ptr-4(cs285 [PTR-4::mCherry])* were generated using the SapTrap method (Schwartz and Jorgensen 2016). Briefly, *ptr-4* single-guide RNA (TTTCTAGAGTCGGGGTGAAA) was inserted into the Cas9 expression plasmid pDD162 (Dickinson *et al.* 2013) and coinjected with a plasmid derived from the plasmid pMLS279 and containing *ptr-4* homology arms attached to SfGFP or mCherry (Schwartz and Jorgensen 2016). Both *ptr-4(cs264 [PTR-4::SfGFP])* and *ptr-4(cs285 [PTR-4::mCherry])* animals were viable and appeared normal (*cs264*: *n* = 93/96 normal, 3/96 unaccounted for), indicating the tag does not interfere with function. To generate *ptr-4(cs273)*, *ptr-4* single-guide RNA (AGGAATCGAAAGAACTGTGA) was injected with recombinant Cas9 protein (University of California, Berkeley) and marker pRF4 [*rol-6(su1006)*], after (Dokshin *et al.* 2018). Heterozygous *cs273* animals were recognized based on progeny embryonic lethality; the mutant allele was recovered over *szT1* and then rescued by a *ptr-4* transgene. *ptr-4(cs279)* arose during an attempted ZF (degron) tagging experiment (Armenti *et al.* 2014) using the single-guide RNA that generated *ptr-4(cs264[PTR-4::SfGFP])* and the recombinant Cas9 protein and marker pRF4 used to generate *ptr-4(cs273)*; homozygous *cs279* animals were recognized based on their mild short and fat (Dpy) body shape. Edits in all alleles were determined by Sanger sequencing of genomic PCR products.

RNAi
J.D.C. initially identified *ptr-4* in a candidate-based RNAi screen for genes required for LET-653(ZP) localization. Subsequent follow-up experiments confirmed this finding. For Figures 1, 3, and 7, *ptr-4* double-stranded RNA (dsRNA) was synthesized using the Ambion MEGAscript RNAi Kit (AM1626; Ambion) and injected into gravid hermaphrodites. Templates used were *ptr-4* RNAi bacterial clone C45B2.7 (Ahringer; *ptr-4* RNAi 1) and genomic DNA amplified with primers oJC259 (TAATACGACTCACTATAGGG CGTCTTAGCGACTATGGTAAAC) and oJC243 (TAATACGACTCAC TATAGGGCGTGGTTTTAATGATTTCCAGC; *ptr-4* RNAi 2). For vulva aECM experiments, embryos laid 1–48 h after injection were collected and observed 48–72 h later. Mock controls used dsRNA derived from the empty vector (EV) clone L4440 (Kamath and Ahringer 2003). All other RNAi experiments were done by feeding animals bacteria expressing dsRNA (Timmons *et al.,* 2001). *ptr-4*, *rab-5*, *rab-7*, and *rab-11* RNAi were carried out using sequenced and confirmed clones from the Ahringer library; as mock nontargeting dsRNA from the Ahringer library clone Y95B8A_84.g was used.

Staging and microscopy
Embryos were selected at the 1.5-fold stage and then incubated for the number of hours indicated before mounting for imaging. L4 larvae were staged by vulva morphology. Live worms were immobilized with 50 mM levamisole in M9 and mounted on a slide with 2% agarose.
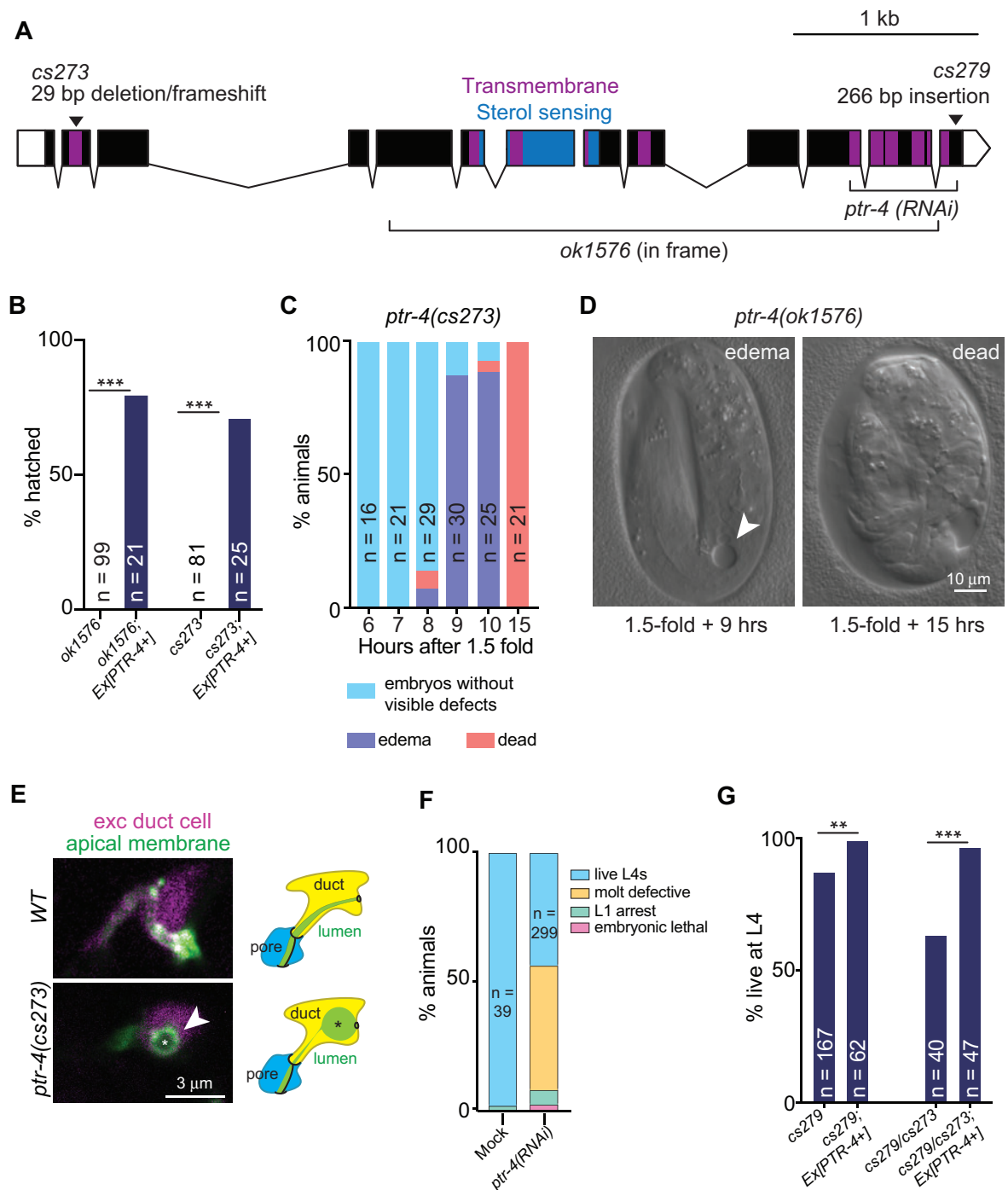
Figure 1 *ptr-4* null mutants are embryonic lethal. (A) *ptr-4* gene model with the transmembrane domains indicated in purple. Five of the 12 predicted TM domains (TmPred; Hofmann and Stoffel 1993) comprise the SSD (blue), a domain also found in some non-PTR proteins that bind cholesterol (Kuwabara and Labouesse 2002). The studied mutations and target of the RNAi are indicated. *ok1576* is a 3093-bp in-frame deletion that removes the SSD and 9 transmembrane domains. We used CRISPR/Cas9 to generate *cs273*, which is a 29-bp deletion causing a frameshift and early stop within the first transmembrane domain (see also Supplementary Figure S1). *cs279* is a 266-bp insertion at the *ptr-4* 3′ end containing unrelated sequences derived from the genes *rol-6* and *pie-1* (see also Supplementary Figure S1). *cs279* is predicted to delete the last three amino acids of PTR-4 and replace them with 17 unrelated amino acids before a new stop codon that is then followed by 213 additional nucleotides before the endogenous stop codon; this extended 3′ UTR may interfere with normal gene expression. (B) *ptr-4* mutants of either allele failed to hatch and were rescued by a large genomic fragment containing the normal *ptr-4* gene. ***P < 0.0001, Fisher's exact test. (C) In *ptr-4(cs273)* mutants, edemas form in the hours after the 1.5-fold stage, and eventually, the embryos die without hatching. (D) DIC images of *ptr-4(ok1596)* embryos at the indicated timepoints. Arrowhead indicates edema. (E) Edema formed within the excretory duct tube lumen. Confocal images of *wild type (WT)* and *ptr-4(cs273)* mutants with the duct cytoplasm marked with *lin-48pro::mRFP* and the apical membrane marked with *RDY-2::GFP*. Schematic interpretations of the phenotype are shown at right. (F) *ptr-4(cs279)* is a hypomorph. Many *cs279* mutants survive but larval lethality is enhanced in *cs279/cs273* trans-heterozygotes. To assess trans-heterozygote survival, *cs279* males were crossed to *cs273; Ex[PTR-4+]* hermaphrodites and their nontransgenic progeny were scored for lethality. *cs279* lethality is rescued by a large genomic fragment containing *ptr-4*. ***P < 0.0001, **P < 0.001, Fisher's exact test. (G) Many *ptr-4(RNAi)* larvae died due to incomplete molting with small fractions dying as very small L1 larvae (L1 arrest) or as embryos.

For experiments in Figures 1, 4, and 5, C and D, fluorescent and differential interference contrast (DIC) images were captured on a compound Zeiss Axioskop fitted with a Leica DFC360 FX camera. Images were processed and merged using ImageJ.

For experiments in Figures 2 and 5, A, B, and E, worms were imaged with ORCA-flash 4.0 camera (Hamamatsu) mounted on an Axio Imager.M2 fluorescence microscope with a 63x Plan-Apochromat objective (Carl Zeiss, Germany) and an HXP 120 C light source using ZEN 2.6 software. All images were adjusted to the same parameters with OMERO.web 5.3.4-ice36-b69. For COL-19::GFP and DAPI staining, worms were imaged with an Olympus Fluoview FV3000 system with PTM voltage = 500, with an objective 60x 1.3 NA with silicone oil.

DAPI staining was performed according to Moribe *et al.* (2004), with minor modifications. For staining, we used 10 μg/μl of DAPI in M9. Animals were analyzed by fluorescence microscopy for DAPI staining in nuclei.

For Figure 6B, Structured illumination microscopy (SIM) was done with DeltaVision OMX Optical Microscope (version 4), Software: DeltaVision OMX softWoRx. Four hundred and eighty-eight488 laser was used at 10%, exposure time was 100 ms, with 95 MHz. Oil 1.518. Image reconstruction was done with software in the Softworx software (GE Healthcare) with a Wiener filter setting of 0.008. K0 angle −0.7895550 Bias Offset 30. Image were analyzed in OMERO.web 5.3.4-ice36-b69.

For experiments in Figures 6D and 7, images were captured with a Leica TCS SP8 confocal microscope. For experiments in Figures 3 and 7, A and B, images were captured with a Leica DMi8 confocal microscope. Images were processed and analyzed using ImageJ. To measure LPR-3 or LET-653 fluorescence intensity, a 10-pixel thick line was drawn across the vulva lumen at the designated cell region. A single focal plane of the vulva midline was chosen for analysis from confocal z stack images of L4.4–L4.5 stage animals. For LPR-3, the two peak GFP fluorescence values corresponding to the apical membrane at each side of the lumen were recorded for each animal. For LET-653(ZP), the average fluorescence intensity in the three microns closest to each apical membrane peak fluorescence was divided by the average fluorescence in the center of the vulva to construct a ratio. Individual fluorescence intensity peak values or ratios were plotted in GraphPad Prism8.

Swimming test

Young adults were placed on M9 buffer for 5 s. The body bends were counted for 30 s. At least eight worms of each condition were analyzed per experiment, and the experiment was performed three times. The results are presented as the average of tail movements per 30 s. The data were analyzed with a one-tail ANOVA followed by Dunnett's multiple comparisons test in Prism 7.

Transmission electron microscopy

For transmission electron microscopy (TEM), *C. elegans* animals were transferred to a droplet of M9 medium on a 100-μm cavity of a 3-mm aluminum specimen carrier (Engineering office M. Wohlwend GmbH, Sennwald, Switzerland). Five to 10 worms were added to the droplet and the excess M9 medium was sucked off with dental filter tips. A flat aluminum specimen carrier was dipped in 1-hexadecene and added on top. Immediately, the specimen carrier sandwich was transferred to the middle plate of an HPM 100 high-pressure freezer (Leica Microsystems, Vienna, Austria) and frozen immediately without using ethanol as synchronizing medium.

Freeze-substitution was carried out in water-free acetone containing 1% OsO_4 for 8 h at −90°C, 7 h at −60°C, 5 h at −30°C, 1 h at 0°C, with transition gradients of 30°C/h, followed by 30 min incubation at room temperature . Samples were rinsed twice with acetone water-free, block-stained with 1% uranyl acetate in acetone (stock solution: 20% in MeOH) for 1 h at 4°C, rinsed twice with water-free acetone, and embedded in Epon/Araldite (Merck, Darmstadt, Germany): 66% in acetone overnight, 100% for 1 h at RT and polymerized at 60°C for 20 h. Ultrathin sections (50 nm) were poststained with Reynolds lead citrate and imaged in a Talos 120 transmission electron microscope at 120 kV acceleration voltage equipped with a bottom-mounted Ceta camera using the Maps software (Thermo Fisher Scientific, Eindhoven, the Netherlands).

Results

PTR-4 is essential for embryo hatching and for maintenance of lumen diameter within the excretory duct tube

ptr-4 is one of many *ptr* genes previously shown to be essential for molting (Zugasti *et al.* 2005). To define *ptr-4* functions, we examined *ptr-4* mutants. Using CRISPR/Cas9, we generated a new putative null allele of *ptr-4*, *cs273*. This allele has a 23-bp deletion that disrupts the first predicted transmembrane domain of PTR-4, followed by a frameshift and early stop (Figure 1A). We also obtained another deletion allele, *ok1576*, from the knockout consortium (Moerman and Barstead 2008); *ok1576* contains a 2.2-kb in-frame deletion that removes most of the PTCHD but leaves the first and last transmembrane domains intact (Figure 1A). Both alleles were 100% embryonic lethal (Figure 1B). Both were efficiently rescued by a large genomic fragment containing the *ptr-4* gene (Figure 1B), indicating that lethality was indeed caused by loss of *ptr-4*.

Upon closer inspection, we found that *ptr-4* mutant embryos had defects in hatching and in maintaining lumen diameter within tubes of the excretory system. *ptr-4* mutant embryos appeared normal until the time period when they should hatch (Figure 1C). Hatching never occurred, however, suggesting a defect in eggshell dissolution. Embryos subsequently developed edemas that began as large dilations within the lumen of the excretory duct tube, a narrow unicellular tube that is required for fluid excretion (Figure 1, C–E). By 15 h after the expected time of hatch, all embryos were dead (Figure 1, C and D). Notably, both the hatching defect and excretory phenotypes of *ptr-4* mutants resemble defects observed in mutants lacking the lipocalin LPR-3 (a putative lipid transporter) or various other known precuticle aECM components that line the epidermis and/or the duct tube channel (Hishida *et al.* 1996; Stone *et al.* 2009; Mancuso *et al.* 2012; Gill *et al.* 2016; Forman-Rubinsky *et al.* 2017; Pu *et al.* 2017; Cohen *et al.* 2019).

PTR-4 is required for proper cuticle patterning and permeability barrier formation

To examine requirements for *ptr-4* at stages later than embryogenesis, we turned to RNAi and to a hypomorphic allele, *cs279* (described below). *ptr-4(RNAi)* caused relatively minor embryonic or early larval lethality, but about 50% of the animals had molting defects similar to those described previously (Zugasti *et al.* 2005; Figure 1F). The remaining animals progressed to adulthood but were small (Figure 2A), uncoordinated (Figure 2B), and showed cuticle defects as described below. In *C. elegans*, locomotion requires alternating contraction of body wall
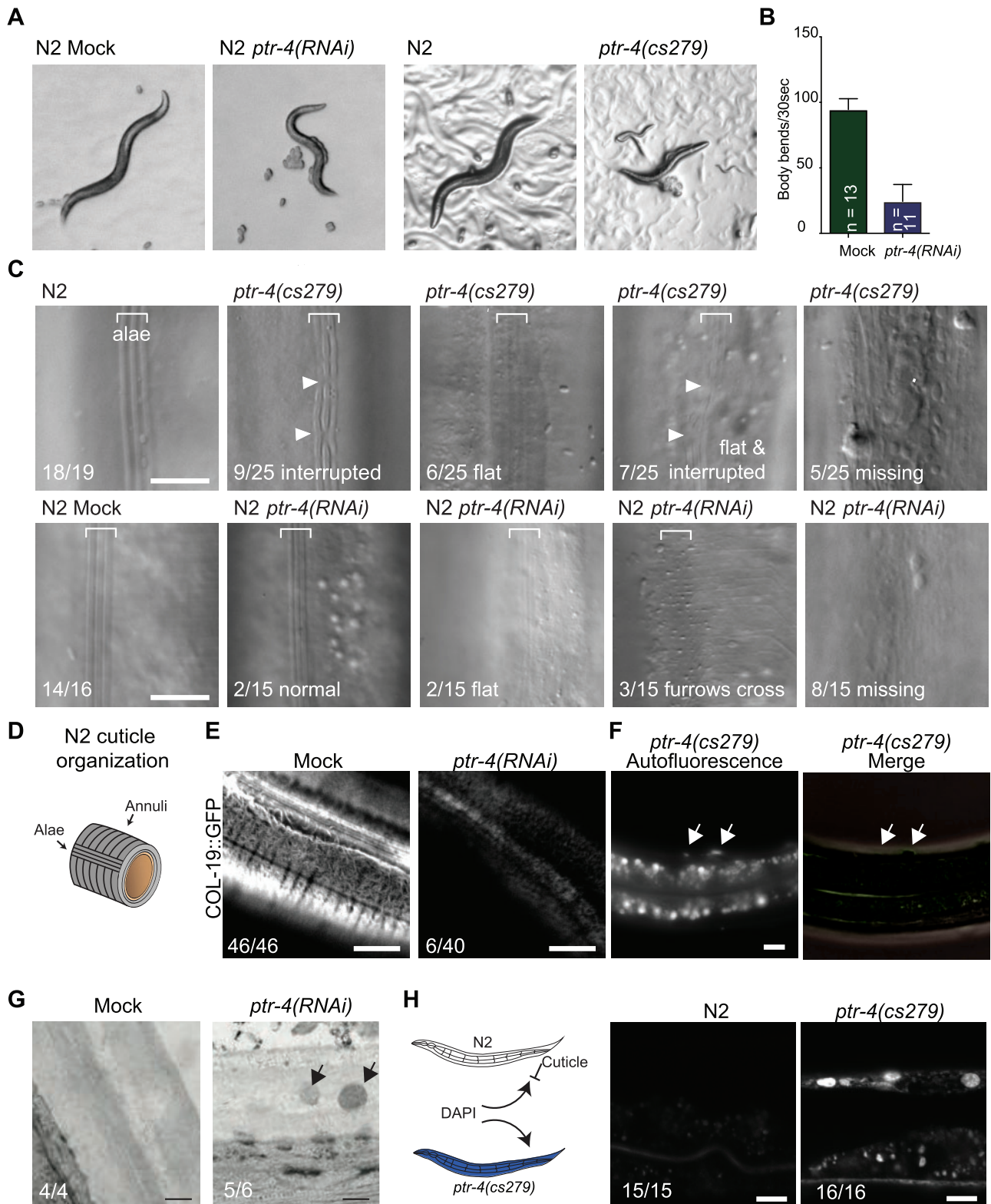
Figure 2 PTR-4 depletion induces cuticular defects. (A) *ptr-4(cs279)* and *ptr-4(RNAi)* adults are small and uncoordinated. (B) Mock treated and *ptr-4(RNAi)* worms were placed in M9 media and were allowed to swim. Body bend analysis in a 30-s test showed reduced motility upon *ptr-4(RNAi)*. (C) DIC images of N2 and *ptr-4(cs279)* worms. The cuticle in *ptr-4(cs279)* and *ptr-4(RNAi)* worms is structurally impaired with multiple types of alae defects. Arrowheads indicate alae interruptions. (D) Schematic depiction of the cuticle with annuli and alae. (E) PTR-4 loss disrupts COL-19::GFP localization. COL-19::GFP marked annuli in all wild-type adults, but was undetectable in 34/40 *ptr-4(RNAi)* adults. (F) *ptr-4(cs279)* animals have abnormal packets of autofluorescent material within the cuticle. (G) TEM images from the mid-body, showing cuticle structure in Mock and *ptr-4(RNAi)* treated animals. In *ptr-4(RNAi)* animals, some vesicular-like structures were observed within the cuticle. Scale bar, 150 nm. (H) Permeability test using the impermeable dye DAPI. In animals with an intact cuticle DAPI is not able to infiltrate and stain cell nuclei. *ptr-4(RNAi)* makes the cuticle permeable. Representative DAPI images of N2 or *ptr-4(cs279)* animals upon incubation with DAPI. Scale bar, 10 μm.
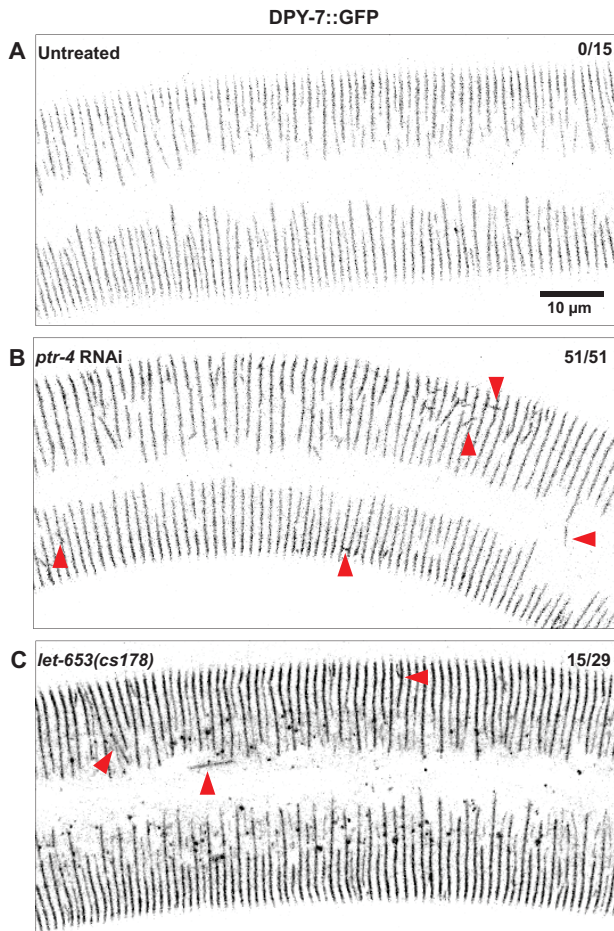
Figure 3 *ptr-4* is required for proper localization of the early cuticle collagen DPY-7. (A) DPY-7::GFP (*qxIs722*) marks circumferential furrows in the L4 cuticle over hyp7. (B) *ptr-4(RNAi)* caused frequent misoriented furrows (red arrowheads; *n* = 52/52 animals with at least one, and usually multiple, furrows that crossed into an adjacent furrow; *P* < 0.0001, Fisher's exact test). Eleven out of 52 animals had at least one completely longitudinal furrow that crossed 3–5 others; 3/52 animals had a furrow extending across the seam midline. (C) Loss of precuticle factor LET-653 also caused misoriented furrows (*n* = 15/29 animals; *P* = 0.0005, Fisher's exact test). Five out of 29 animals had at least one completely longitudinal furrow that crossed 3–5 others; none had a furrow extending across the seam midline. An excretory duct-specific rescue transgene (*csEx766*) was used to obtain surviving *let-653(cs178)* mutants for observation. In all panels, maximum intensity projections of 10 confocal z-slices from mid-L4 animals are shown. Images are inverted for clarity. Scale bar, 10 μm.

muscles that are connected to the cuticle (Page and Johnstone 2007). In addition, the cuticle has to maintain osmolarity and turgor pressure to consequently achieve movement (Moribe *et al.* 2004). It is likely therefore that cuticle defects contribute to the observed defects in locomotion.

We inadvertently generated the allele *ptr-4(cs279)* when attempting to tag the locus with a degron using CRISPR/Cas9. *cs279* contains a 266-bp insertion of DNA from the genes *rol-6* and *pie-1* inserted just before the *ptr-4* stop codon; this is predicted to modify both the protein and the 3' UTR (Figure 1A and Supplementary Figure S1). Most *ptr-4(cs279)* animals survived (Figure 1G) but were small and uncoordinated, resembling the *ptr-4(RNAi)* adults above (Figure 2A). To confirm that *cs279* is hypomorphic, we demonstrated that its mild lethality is rescued by a large genomic fragment containing *ptr-4* (Figure 1G). Next,
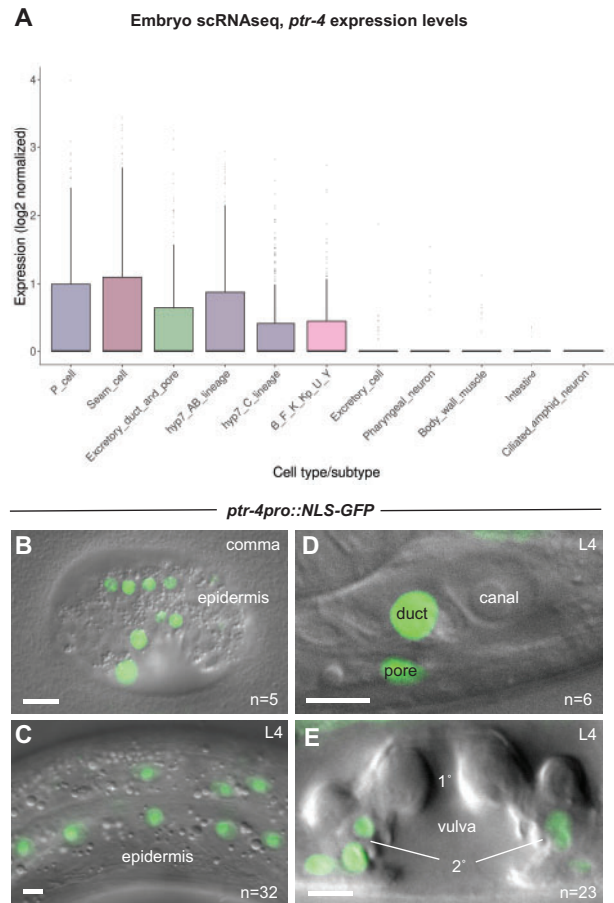

Figure 4 *ptr-4* is expressed in external epithelia. (A) *ptr-4* expression levels across embryonic cell types, as detected by scRNAseq (Packer *et al.* 2019). Data were downloaded and visualized using https://cello.shinyapps.io/celegans_explorer/ (B–E) A *ptr-4pro::NLS-GFP* transcriptional reporter is expressed in developing external epithelia from embryonic to L4 stages. (B) Epidermal cells of bean-stage embryo. (C) Epidermal cells of L4 larva. (D) Excretory duct and pore cells of L4 larva. (E) 2°-lineage-derived cells in the L4 vulva tube. Scale bar, 5 μm.

we generated compound heterozygotes that contained the *ptr-4(cs279)* allele over the *ptr-4(cs273)* null allele. These worms had increased postembryonic lethality compared to *cs279* homozygotes (Figure 1G). Together, these data indicate that *cs279* is a mild hypomorphic allele.

Surviving *ptr-4(cs279)* and *ptr-4(RNAi)* adults had abnormal cuticle structure. The adult epidermal cuticle is organized into circumferential ridges (annuli) that cover the bulk of the epidermis, and longitudinal ridges (alae) that cover the lateral seam cells (Page and Johnstone 2007; Figure 2, C and D). Animals with reduced *ptr-4* activity displayed a variety of alae defects, ranging from interrupted alae to almost complete absence of alae (Figure 2C). Furthermore, the adult-specific collagen COL-19::GFP (Thein *et al.* 2003) was depleted or lost from the cuticle (Figure 2E). By light microscopy, patches of autofluorescent material were observed within the epidermal cuticle (Figure 2F). These abnormal structures in *ptr-4(RNAi)* animals were also observed by TEM (Figure 2G), and closely resembled structures previously reported for mutants of the precuticle factor LET-4 (Mancuso *et al.* 2012). Finally, we found that, similar to some precuticle or cuticle mutants (Mancuso *et al.* 2012; Forman-Rubinsky *et al.* 2017; Cohen *et al.* 2020b; Sandhu *et al.* 2021), the cuticle in *ptr-4(RNAi)*
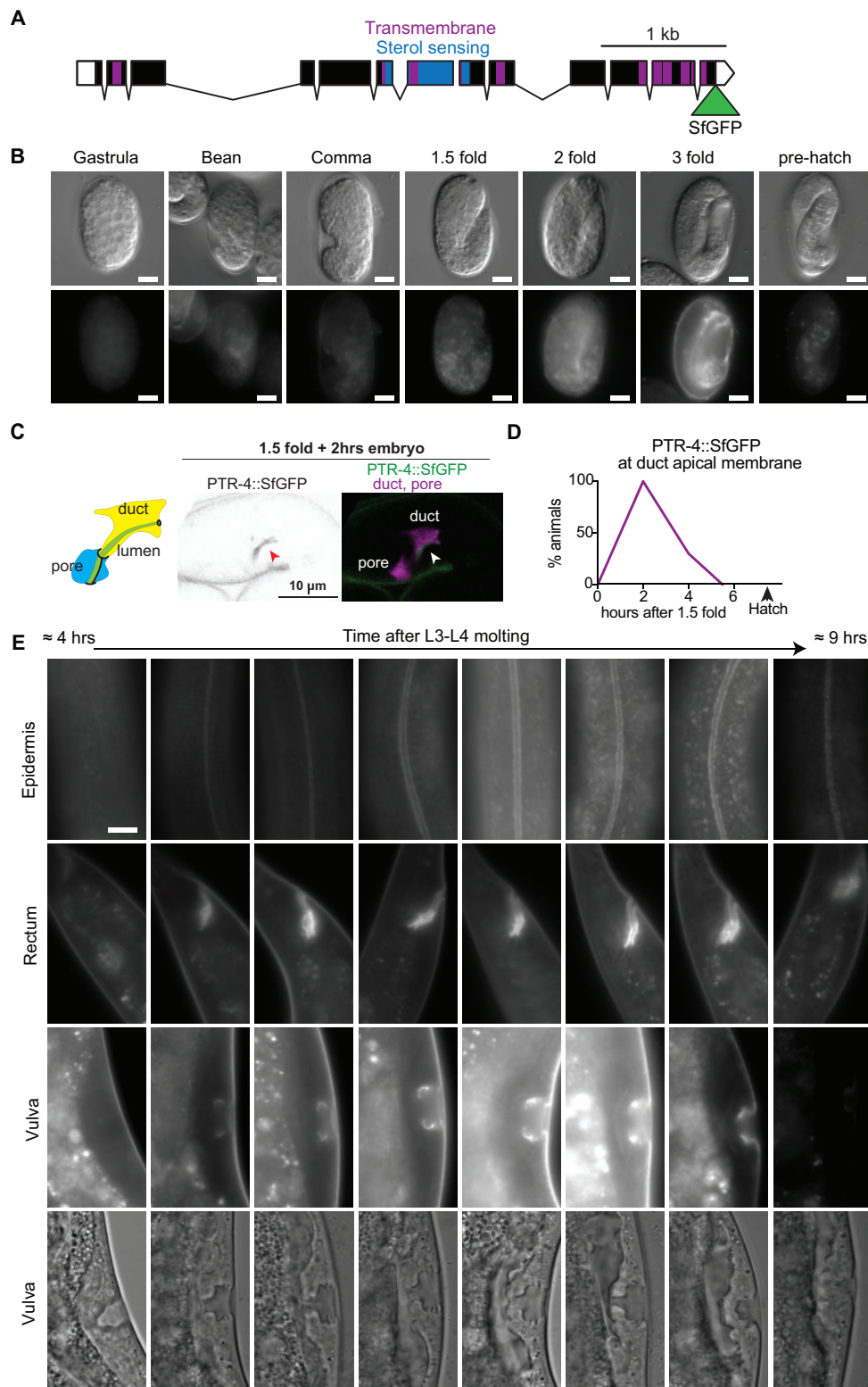
Figure 5 PTR-4 localizes transiently to apical surfaces of external epithelia. (A) *ptr-4* gene model with the transmembrane domains indicated in purple and SSD in blue. Superfolder GFP (SfGFP) was inserted into the *ptr-4* endogenous locus via CRISPR/Cas9 technology to make *ptr-4(cs264 [PTR-4::SfGFP])*. (B) PTR-4::SfGFP localization during worm embryonic development. PTR-4::SfGFP first becomes visible at the twofold stage in the epidermis, rectum, and excretory duct/pore and then disappears before hatching. Scale bar, 10 μm. (C) PTR-4::SfGFP localizes to the apical surface of the excretory duct tube (arrowhead) at 1.5-fold + 2-h embryonic stage. For visualization, the duct and pore cells were labeled with *grl-2pro::mRFP*. (D) Time course of PTR-4::SfGFP expression on the duct apical membrane (*n* = 20 per timepoint). (E) PTR-4::SfGFP localization in L4 substaged larva (*n* = 5 or more per timepoint). PTR-4::SfGFP expression in the epidermis, rectum, and vulva was dynamic during development. While in early L4, there is no PTR-4::SfGFP signal, in mid-L4 it can be observed at the plasma membrane. In late L4 animals, PTR-4::SfGFP localizes to internal structures and prior to molting the signal disappears. Scale bar, 10 μm.
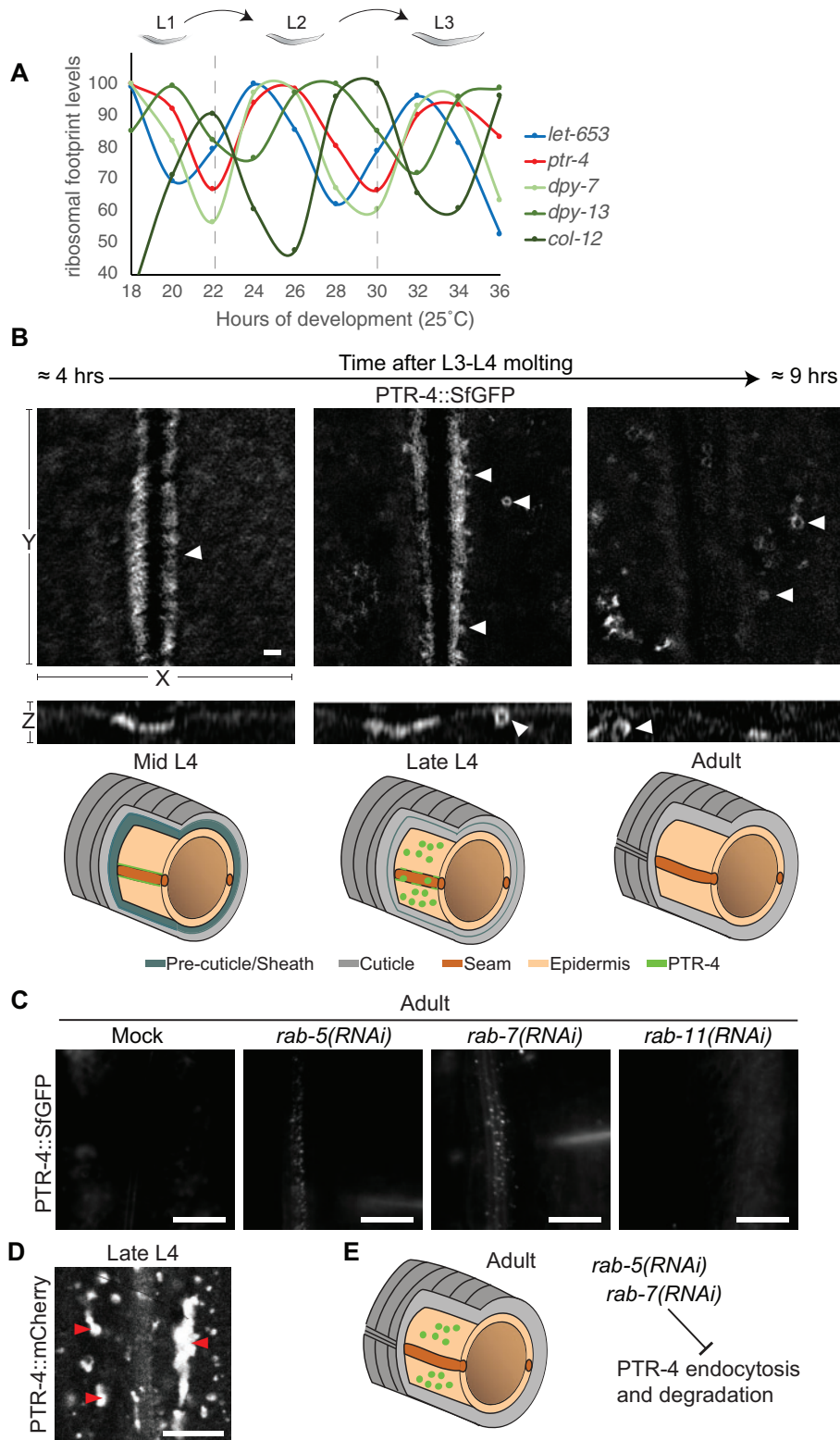
Figure 6 PTR-4 dynamic localization is regulated by endocytosis. (A) PTR-4 ribosomal footprints oscillate during larval development, with peaks coinciding with those of the earliest cuticle collagens. LET-653, DPY-7, DPY-13, and COL-12 are shown as representatives of precuticle and early, intermediate, or late collagens, respectively (Page and Johnstone 2007). Data are extracted from a previously published dataset (Hendriks _et al._ 2014). (B) Structural illumination (SIM) images of PTR-4::SfGFP in the epidermis. In mid-L4 worms, PTR-4::SfGFP is present at the plasma membrane between the seam and hyp7 ($n = 6$). As development proceeds, PTR-4::SfGFP gathers in membrane invaginations ($n = 6$). At late L4 stages, PTR-4::SfGFP localizes exclusively in intracellular compartments ($n = 5$). Scale bar, 1 μm. Schematics below (adapted from Katz _et al._ 2018) summarize the observed changes in PTR-4 localization. (C) PTR-4 localization changes during development are due to endocytosis. RNAi of _rab-5_ ($n = 17/19$) or _rab-7_ ($n = 13/14$) blocked endocytosis and/or degradation, leading to accumulation of PTR-4 within the epidermis of adult worms, whereas 0/10 mock-treated animals and only 1/15 _rab-11_ RNAi animals had detectable PTR-4 at this stage. (D) Unlike PTR-4::SfGFP, PTR-4::mCherry accumulates within large lysosome-like structures in hyp7 (arrowheads; $n = 21/21$ L4s). (E) Model and summary of Rab RNAi results.
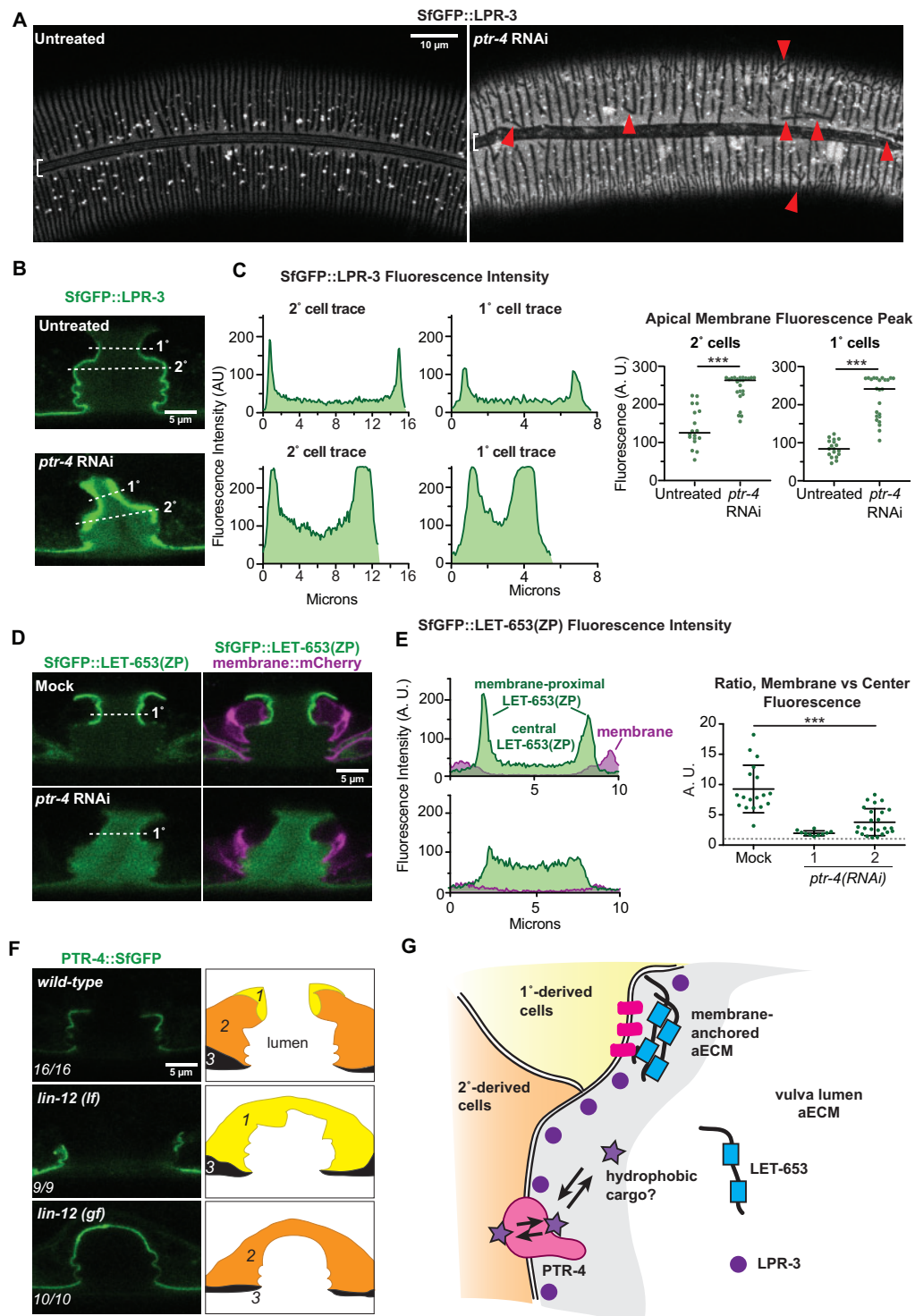
Figure 7 PTR-4 is required for proper assembly of the vulva precuticle matrix. (A and B) LPR-3 accumulates aberrantly at hypodermal and vulva cell apical surfaces after *ptr-4* knockdown. (A) LPR-3 transiently marks alae- and annuli-like bands at L4.5 and L4.6 stages. *ptr-4* RNAi disrupted the alae pattern [control *n* = 14/15 with intact alae, *ptr-4(RNAi)* *n* = 2/9 with intact alae; *P* = 0.0007, Fisher's exact test] and led to consistently brighter LPR-3 signal over hyp7. The annuli-like structures are somewhat branched and irregularly spaced even in control animals, but never longitudinal. However, 5/6 *ptr-4(RNAi)* animals with well-defined patterns showed longitudinal furrows (red arrowhead). (B) At the L4.4 stage, LPR-3 marks all vulva apical surfaces in both control and *ptr-4(RNAi)* animals [control *n* = 9; *ptr-4(RNAi)* *n* = 12]. (C) Quantification of data shown in (B). ***P < 0.0001, Mann–Whitney *U*-test. (D) Localization of LET-653(ZP) to 1˚-derived vulE and vulF cell surfaces is dependent on PTR-4. Knockdown of PTR-4 does not impair secretion of LET-653(ZP), but the integration into the ECM is impaired. (E) Quantification of data shown in (D). Control *n* = 18; *ptr-4(RNAi)* 1 *n* = 10. *ptr-4(RNAi)* 2 *n* = 24. ***P < 0.0001, Mann–Whitney *U*-test. (F) PTR-4::SfGFP is expressed at apical membranes of cells derived from 2˚ or 3˚ lineages, and not in vulE/F cells derived from 1˚ lineages. *lin-12/Notch* mutations were used to alter cell fates as indicated in schematics (Greenwald *et al.* 1983). (G) Models: PTR-4 may import or export a hydrophobic cargo (star) that impacts aECM assembly. For example, PTR-4 may import a cargo such as LPR-3 to restrict its levels throughout the aECM, and abnormally high levels of this cargo may perturb the incorporation of other matrix factors such as LET-653(ZP). Alternatively, PTR-4 may export an unknown cargo that both restricts LPR-3 accumulation and facilitates LET-653(ZP) assembly on neighboring cells.

animals was permeable to small molecules (Figure 2H), indicating that the permeability barrier was defective.

ptr-4 mutants show altered localization of the early cuticle collagen DPY-7

A recent survey of cuticle collagens found that only six (DPY-2, DPY-3, DPY-7, DPY-8, DPY-9, and DPY-10) are required for maintaining cuticle barrier function (Sandhu *et al.* 2021). These collagens are amongst the earliest expressed and incorporated during the molt cycle (Hendriks *et al.* 2014) and are required for the pattern of annular furrows (McMahon *et al.* 2003). To test if *ptr-4* affects such early collagens, we examined the localization of a previously described DPY-7::GFP translational reporter that normally marks the cuticle furrows (Miao *et al.* 2020). In wild-type animals, DPY-7::GFP furrows are circumferential and nonintersecting, and they terminate before reaching the seam (Figure 3A). In *ptr-4(RNAi)* animals, DPY-7::GFP still marked cuticle furrows, but many furrows showed abnormal shifts in orientation, with some crossing into adjacent furrow regions or even appearing perpendicular to the others (Figure 3B). In rare cases, furrows also extended into the seam cell region (Figure 3B). Similar but somewhat less penetrant defects were seen after loss of the precuticle component LET-653 (Figure 3C). Therefore, *ptr-4* depletion affects a very early step of cuticle patterning.

ptr-4 is widely expressed in cuticle-lined epithelia

To determine which cells express *ptr-4*, we first analyzed published single-cell RNA sequencing (scRNAseq) data (Packer *et al.* 2019). Embryonic scRNAseq data showed *ptr-4* most highly expressed in epidermal cell types and in tubular epithelia such as the rectum and the excretory duct and pore (Figure 4A). Notably, all of these tissues are lined first by precuticle and then by cuticle. Very little or no *ptr-4* expression was detected in noncuticle-lined internal epithelia such as the intestine or excretory canal tube, or in other tissue types such as muscle or neurons.

We then generated a *ptr-4* transcriptional reporter using 1.6 kb of the upstream regulatory region to drive nuclear-localized GFP expression. Consistent with the scRNAseq data, this reporter showed broad expression in external epithelia, beginning at the bean stage of embryogenesis and continuing throughout development (Figure 4, B–E). The expression did show some temporal and cell-type specificity, however; for example, in the vulva tube, expression began only after initial lumen formation and was seen in only 2°-lineage-derived cells but not 1°-lineage-derived cells (Figure 4E, see also below).

In summary, *ptr-4* is expressed in most but not all external epithelia, starting at the time period when precuticle is first synthesized.

PTR-4 localizes transiently to the apical plasma membrane of outward-facing epithelia

To determine when and where PTR-4 protein localizes, we used CRISPR/Cas9 to tag endogenous PTR-4 with the fluorescent protein Superfolder (Sf) GFP (Pedelacq *et al.* 2006; Figure 5A). PTR-4::SfGFP was not detected during the early part of embryogenesis but appeared by the twofold stage along the apical membranes of the epidermis, excretory duct and pore, and rectum (Figure 5, B and C). However, PTR-4 expression was transient and rapidly cleared prior to hatching (Figure 5, B and D). PTR-4 reappeared in the middle of each subsequent larval stage, during the time when precuticle is present (Gill *et al.* 2016; Forman-Rubinsky *et al.* 2017; Cohen and Sundaram 2020). During L4 stage, the stage preceding adulthood, PTR-4 was present on apical surfaces between

the major epidermis (hyp7) and the lateral seam cells (Figure 5E), which secrete alae (as well as precuticle factors that are needed to shape alae; Liégeois *et al.* 2006; Kolotuev *et al.* 2009; Forman-Rubinsky *et al.* 2017; Cohen *et al.* 2019; Flatt *et al.* 2019). PTR-4 was also present along apical surfaces of the rectum and of some cells in the vulva, the tube through which eggs will be laid (Figure 5E). As in embryogenesis, PTR-4 was transient and disappeared as the adult cuticle was made. Together, these observations demonstrate that PTR-4 is present on the apical surfaces of external epithelia during the time period when precuticle is present.

PTR-4 transient plasma membrane localization is regulated by oscillating protein translation and endocytosis

Cellular protein concentration is dependent on protein synthesis and degradation. To investigate the mechanisms controlling PTR-4 plasma membrane expression, we first analyzed published transcriptional profiling and ribosomal footprint data during larval development (Hendriks *et al.* 2014). Both *ptr-4* mRNA levels and ribosome occupancy oscillated during development with peaks during intermolts and troughs during molting (Figure 6A). This oscillatory behavior is also shared by most aECM-encoding genes, with precuticle factors (e.g. LET-653) and some of the earliest cuticle collagens, such as DPY-7, peaking slightly before or at the same time as PTR-4, and most cuticle collagens peaking later (Figure 6A).

Next, we determined how PTR-4 clearance might be regulated. To this end, we aimed to follow changes in PTR-4 plasma membrane localization in the epidermis, using SIM (Figure 6B). After the L3–L4 molt, PTR-4 was localized at the apical plasma membranes between hyp7 and the seam cells. In mid-L4, PTR-4 started to move away from this contact site and sites of PTR-4 endocytosis were observed. At the early adult stage, PTR-4 was absent from the contacts between epidermis and seam cells. If PTR-4 was indeed endocytosed and then degraded in the lysosome, interfering with this pathway should stabilize PTR-4. When we knocked-down the key endocytic regulators RAB-5 and RAB-7, PTR-4 still moved away from the epidermis-seam cell contact but was no longer efficiently cleared, and instead persisted into adulthood (Figure 6C). In contrast, knockdown of the recycling factor RAB-11 had no such effect (Figure 6C). Finally, we observed that a PTR-4::mCherry fusion accumulated strongly within lysosome-like structures prior to disappearing (Figure 6D), suggesting that PTR-4::SfGFP disappearance was due at least in part to fluorophore quenching within an acidic compartment.

In summary, our data indicate that PTR-4 transient plasma membrane expression is regulated through oscillating PTR-4 protein synthesis on one hand and endocytosis and likely lysosomal degradation on the other hand (Figure 6E).

PTR-4 is required to limit the accumulation of the lipocalin LPR-3 and to properly localize the ZP protein LET-653 in the vulva precuticle

The similarity of *ptr-4* mutants to known precuticle mutants and the spatial and temporal pattern of PTR-4 localization are consistent with a possible role in precuticle assembly or remodeling. To test this hypothesis, we examined the localization of several precuticle factors, including the lipocalin LPR-3 and the ZP domain protein NOAH-1. Both LPR-3 and NOAH-1 normally localize to developing annuli and alae ridges of the nascent adult cuticle (Figure 7A and Supplementary Figure S2; Forman-Rubinsky *et al.* 2017; Vuong-Brender *et al.* 2017; Cohen *et al.* 2020b). After *ptr-4* RNAi knockdown, LPR-3 defined misoriented furrows similar to

those seen above with DPY-7::GFP (Figure 7A). LPR-3 also appeared missing or disorganized over the alae region, but brighter than normal over the annuli (Figure 7A), while NOAH-1 remained relatively faint in both locations (Supplementary Figure S2).

To further test effects on precuticle, we turned to the vulva tube, where different combinations of precuticle factors assemble on the apical surfaces of each different cell type (Cohen *et al.* 2020b). Two distinct types of vulva lineages, 1° *vs* 2°, generate 22 vulva epithelial cells of 7 different types (vulA-vulF). We showed previously that, during mid-L4, LPR-3 initially marks all vulva cell apical surfaces and then later LPR-3 and NOAH-1 mark only ventral, 2° lineage-derived cell surfaces before disappearing (Figure 7B and Supplementary Figure S2); conversely, the secreted ZP domain of LET-653 specifically decorates the apical surfaces of the dorsal-most 1°-lineage-derived vulE and vulF cells (Cohen *et al.* 2020a, 2020b; Figure 7D). When PTR-4 was knocked-down by RNAi, the general LPR-3 and NOAH-1 patterns remained unchanged, but SfGFP::LPR-3 fluorescence intensity was greatly increased over all cell types (Figure 7, B and C, Supplementary Figure S2). In contrast, LET-653(ZP)::SfGFP was no longer concentrated at 1°-derived cell surfaces, but instead filled the entire vulva lumen (Figure 7, D and E). There appeared to be no defect in LET-653 secretion; however, the assembly of LET-653(ZP) in the membrane-proximal ECM was defective.

Importantly, and consistent with the transcriptional reporter data above (Figure 4), PTR-4::SfGFP was never observed on 1° lineage-derived vulE or vulF cells, but rather marked the apical membranes of the more ventral 2° or 3° lineage-derived cells (Figure 7F). Vulva cell-type specificity was further confirmed by examining *lin-12/Notch* mutants with cell fate alternations (Figure 7F). PTR-4::SfGFP expression was reduced in *lin-12* loss-of-function (lf) mutants, which lack 2° vulva lineages, and was expanded in *lin-12* gain-of-function (gf) mutants, which have extra 2° vulva lineages (Figure 7F;Greenwald *et al.* 1983). Based on the expression pattern of PTR-4 relative to the phenotypes observed, we infer that PTR-4 could participate directly in LPR-3 clearance from 2° cell surfaces, but must act cell nonautonomously to limit LPR-3 levels and to promote LET-653 matrix assembly over 1° vulva cells (Figure 7G).

Discussion

The existence of so many *C. elegans* PTR family members has been a long-standing puzzle, given the absence of a canonical Hh signaling pathway. Recent evidence for the regulation of plasma membrane cholesterol levels by PTCH, combined with the homology to bacterial RND transporters, suggests a unifying hypothesis that all PTCHD/PTR proteins are transmembrane pumps for hydrophobic cargos. However, the biological roles that these proteins fulfill remain little characterized. Prior work suggested that many *C. elegans* PTR proteins affect the development of the collagenous cuticle (Zugasti *et al.* 2005; Hao *et al.* 2006a). Here, we provided evidence that *C. elegans* PTR-4 promotes proper assembly of the precuticle, a molecularly distinct aECM that precedes and patterns the cuticle. First, *ptr-4* mutants display a set of phenotypes that closely resemble those of known precuticle mutants. Second, the presence of PTR-4 on apical membranes suggests a role in transporting a small hydrophobic molecule across those membranes, and its oscillatory temporal pattern and restriction to external epithelia are consistent with a role in transporting factors relevant to precuticle synthesis. Third, PTR-4 is required to limit the levels of at least one specific precuticle

aECM factor, the lipocalin LPR-3, and to promote proper matrix incorporation (though not secretion) of another precuticle aECM factor, the ZP protein LET-653. Finally, we note that there is prior TEM evidence for a role of the PTR DAF-6 in organizing the aECM of glial sheath and socket tubes (Perens and Shaham 2005; Oikonomou *et al.* 2011). Given the varied types of aECM that are present on different epithelial surfaces and at different stages of the *C. elegans* life cycle (Cohen and Sundaram 2020), it is plausible that the large family of *C. elegans* PTR proteins is dedicated to transporting different types of lipids and small molecules that contribute (directly or indirectly) to these diverse aECMs.

Relationship of PTR-4 to the eggshell, precuticle, and cuticle aECMs

The precuticle is a transient aECM that covers developing epithelia prior to and during early stages of cuticle collagen deposition and maturation (Cohen and Sundaram 2020). The precuticle also sits at the interface of the embryo and the inner eggshell. The *ptr-4* mutant phenotypes described here suggest defects in all three of these distinct aECMs (the eggshell, precuticle, and cuticle). This could reflect multiple distinct roles for PTR-4, or all of the defects could be explained by a common role, such as a role in precuticle assembly and remodeling.*ptr-4* and *lpr-3* are not expressed until long after the eggshell forms, and mutants do not exhibit early developmental defects characteristic of eggshell mutants (Stein and Golden 2018), so failure to disassemble the eggshell in these mutants is unlikely to reflect a problem in the main eggshell structure itself. Potentially, the innermost layer of the eggshell could be impacted by the aberrant formation of the precuticle matrix beneath it, leading to hatching defects. Alternatively, eggshell disassembly may require specific "I'm ready" signals to be released from the embryonic cuticle, and aberrant cuticle organization could disrupt this communication. Finally, *ptr-4* could be required to synthesize or transport a relevant signal, such as a steroid hormone that triggers hatching. Normal hatching in all known cuticle mutants and the clearance of PTR-4 prior to hatching (Figure 5) make the second two models less likely. The mechanisms that control hatching in *C. elegans* are largely unknown, and *ptr-4* and *lpr-3* should be useful tools for further studies.

We suggest that *ptr-4* cuticle defects could also be an indirect consequence of aberrant precuticle, since the precuticle patterns the cuticle (Cohen and Sundaram 2020). Defects in LPR-3, LET-653(ZP), and DPY-7 collagen localization clearly demonstrate that *ptr-4* loss disrupts the precuticle as well as the deposition pattern of some of the earliest cuticle collagens that replace it. The process by which the precuticle is exchanged for the cuticle is another area that is poorly understood and needs further study.

Models for PTR-4 function in precuticle organization

The most ancient and well-established roles for PTR proteins are as transmembrane pumps for hydrophobic cargos (Figure 7G). Depending on their topology, PTR proteins can transport cargo away from or toward the cell cytoplasm. For example, Dispatched exports Hh out of cells and into the environment (Hall *et al.* 2019), while Npc1 exports cholesterol out of the lysosome lumen and into the cytoplasm (Cologna and Rosenhouse-Dantsker 2019; Pfeffer 2019). The directionality with which Patched transports cholesterol is still debated in the literature (Zhang *et al.* 2018; Hu and Song 2019; Petrov *et al.* 2020), though most data, including our data with *C. elegans* PTC-3 (Cadena del Castillo *et al.* 2019), suggest a cholesterol export function. We

unfortunately failed to achieve good expression of PTR-4 in either *Saccharomyces cerevisiae* or HEK293 cells, making it impossible to check directly for extrusion of cholesterol or other lipid types by PTR-4; therefore, its specific cargo and direction of transport remain unknown. Given the unusually large number of PTR proteins in *C. elegans*, along with the diverse cargos known for related bacterial RND transporters (Nikaido 2018), it is likely that different PTR proteins transport different classes of cargo.

Given the above, combined with the primary location of PTR-4 at apical plasma membranes, the connection of PTR-4 with the precuticle aECM could be at least threefold. First, PTR-4 could regulate the plasma membrane lipid composition in its vicinity, thereby either promoting or reducing the resident time of aECM remodelers at the plasma membrane and/or negatively or positively regulating the secretion of ECM components. Second, PTR-4 could import small lipophilic molecules into cells, possibly helping to clear aECM components such as LPR-3 or to provide building blocks for aECM or steroid hormone production. Third, PTR-4 could extrude lipids or other small lipophilic molecules that are either regulators or actual components of the aECM. For example, candidate PTR-4 cargoes include members of the divergent Hh-like family in *C. elegans*, many of which also are required for proper aECM organization (Bürglin 2008).

A potential role for PTR-4 in lipoprotein import would be consistent with our finding that LPR-3 accumulates aberrantly in *ptr-4* RNAi animals, suggesting that it is not being properly cleared. Lipocalins are small, cup-shaped proteins that transport lipophilic molecules such as sterols in the extracellular environment (Flower 1996; Steinhoff *et al.* 2021). *lpr-3* mutants share hatching, excretory tube, permeability, and molting phenotypes with *ptr-4* mutants (Forman-Rubinsky *et al.* 2017), so abnormal LPR-3 function could explain many of the *ptr-4* mutant phenotypes. Abnormally high levels of LPR-3 could also perturb the incorporation of other matrix factors such as LET-653(ZP). There is no precedent, however, for PTR proteins acting as lipocalin transporters, and it is possible that PTR-4 affects LPR-3 indirectly, such as through changes in other aECM components.

A potential role for PTR-4 in aECM export would be analogous to the roles of MmpL (mycobacterial membrane protein large) RND proteins, which export various complex glycolipids across the inner cell membrane and into the periplasmic space for eventual incorporation into the outer cell membrane or other layers of the mycobacterial cell envelope (Melly and Purdy 2019). Although the lipid content of the precuticle aECM is not known, many aECMs, including the *C. elegans* eggshell and cuticle, do have significant lipid content, which is thought to confer their permeability barrier functions (Blaxter 1993; Olson *et al.* 2012; Schultz and Gumienny 2012; Bai *et al.* 2020; Cohen *et al.* 2020b). When viewed by TEM, the precuticle aECM has an outer, electron-dense layer that could serve as a lipid-rich covering to corral developing membrane-proximal aECM layers and keep them separate from the more dynamic matrix in the central part of tube lumens (Mancuso *et al.* 2012; Gill *et al.* 2016; Cohen *et al.* 2020b) (Figure 7G). Loss of such a layer could allow secreted factors like LET-653 to move away from the membrane too quickly, hampering their local assembly and interfering with mechanisms that normally clear other factors such as LPR-3.

Caenorhabditis elegans PTR proteins and aECMs

Caenorhabditis elegans has many different types of aECMs that contain different protein components and presumably also vary in lipoprotein or lipid composition (Cohen and Sundaram 2020). For example, the pharynx or foregut contains a chitin-based cuticle distinct from the collagenous cuticle of the body, while internal epithelia contain glycocalyx-like matrices whose composition is largely uncharacterized. Our data suggest a role for PTR-4 in proper organization of the precuticle, which is actually a heterogeneous set of matrices that vary somewhat between tissues and life stages and which must be exchanged for the cuticle during the molt cycle. It is possible that at least some of the other PTR proteins required for molting also affect the precuticle. Prior work showed that the PTR protein DAF-6 may be involved in organization of a distinct sensory matrix that lines amphid glia channels and helps shape these tube-like channels and anchor the sensory dendrites within them (Heiman and Shaham 2009; Oikonomou *et al.* 2011). This sensory matrix contains at least one ZP protein, DYF-7 (Heiman and Shaham 2009; Low *et al.* 2019), and it appears to be disorganized and detached from cell surfaces in *daf-6* mutants (Oikonomou *et al.* 2011), perhaps similar to what we observed for LET-653(ZP) in *ptr-4* mutants. Interestingly, scRNAseq data show that several other *ptr* genes are expressed by epithelia that make distinct types of matrices, such as *ptr-19* in pharyngeal myoepithelia, *ptr-11* in the excretory canal cell, or *ptr-24* in the intestine (Packer *et al.* 2019). We suggest that one explanation for the large expansion of PTR proteins in *C. elegans* could be the need to transport different types of lipids and lipoproteins that contribute to the diverse aECMs in these tissues.

Data availability

Strains and plasmids are available upon request. Supplementary Table S1 lists all strains used in this work. The authors affirm that all data necessary for confirming the conclusions of the article are present within the article, figures, and tables.

Supplementary material is available at *GENETICS* online.

Conflicts of interest

The authors declare that there is no conflict of interest.

Literature cited

Armenti ST, Lohmer LL, Sherwood DR, Nance J. 2014. Repurposing an endogenous degradation system for rapid and targeted depletion of *C. elegans* proteins. Development. 141:4640–4647.

Bai X, Huang LJ, Chen SW, Nebenfuehr B, Wysolmerski B, *et al.* 2020. Loss of the seipin gene perturbs eggshell formation in *Caenorhabditis elegans*. Development. 147:dev192997.

Blaxter ML. 1993. Cuticle surface proteins of wild type and mutant *Caenorhabditis elegans*. J Biol Chem. 268:6600–6609.

Brenner S. 1974. The genetics of *Caenorhabditis elegans*. Genetics. 77: 71–94.

Bürglin TR. 2008. Evolution of Hedgehog and Hedgehog-related genes, their origin from Hog proteins in ancestral eukaryotes and discovery of a novel Hint motif. BMC Genomics. 9:127.

Bürglin TR, Kuwabara PE. 2006. Homologs of the Hh signalling network in *C. elegans*. (January 28, 2006), *WormBook*, ed. The *C. elegans* Research Community, WormBook, doi/10.1895/wormbook.1.76.1, http://www.wormbook.org

Cadena del Castillo CE, Hannich JT, Kaech A, Chiyoda H, Fukuyama M, *et al.* 2019. Patched regulates lipid homeostasis by controlling cellular cholesterol levels. bioRxiv. doi:10.1101/816256.

Chaudhry A, Noor A, Degagne B, Baker K, Bok LA, *et al.*; DDD Study. 2015. Phenotypic spectrum associated with PTCHD1 deletions and truncating mutations includes intellectual disability and autism spectrum disorder. Clin Genet. 88:224–233.

Chiyoda H, Kume M, del Castillo CC, Kontani K, Spang A, *et al.* 2021. *Caenorhabditis elegans* PTR/PTCHD PTR-18 promotes the clearance of extracellular Hedgehog-related protein via endocytosis. PLoS Genet. 17:e1009457.

Chung JH, Larsen AR, Chen E, Bunz F. 2014. A PTCH1 homolog transcriptionally activated by p53 suppresses Hedgehog signaling. J Biol Chem. 289:33020–33031.

Cohen JD, Bermudez JG, Good MC, Sundaram MV. 2020a. A *C. elegans* Zona Pellucida domain protein functions via its ZPc domain. PLoS Genet. 16:e1009188.

Cohen JD, Flatt KM, Schroeder NE, Sundaram MV. 2019. Epithelial shaping by diverse apical extracellular matrices requires the nidogen domain protein DEX-1 in *Caenorhabditis elegans*. Genetics. 211:185–200.

Cohen JD, Sparacio AP, Belfi AC, Forman-Rubinsky R, Hall DH, *et al.* 2020b. A multi-layered and dynamic apical extracellular matrix shapes the vulva lumen in *Caenorhabditis elegans*. eLife. 9: e57874.

Cohen JD, Sundaram MV. 2020. *C. elegans* apical extracellular matrices shape epithelia. J Dev Biol. 8:23.

Cologna SM, Rosenhouse-Dantsker A. 2019. Insights into the molecular mechanisms of cholesterol binding to the NPC1 and NPC2 proteins. Adv Exp Med Biol. 1135:139–160.

Dickinson DJ, Ward JD, Reiner DJ, Goldstein B. 2013. Engineering the *Caenorhabditis elegans* genome using Cas9-triggered homologous recombination. Nat Methods. 10:1028–1034.

Dokshin GA, Ghanta KS, Piscopo KM, Mello CC. 2018. Robust genome editing with short single-stranded and long, partially single-stranded DNA donors in *Caenorhabditis elegans*. Genetics. 210:781–787.

Flatt KM, Beshers C, Unal C, Cohen JD, Sundaram MV, *et al.* 2019. Epidermal remodeling in *Caenorhabditis elegans* Dauers requires the nidogen domain protein DEX-1. Genetics. 211:169–183.

Flower DR. 1996. The lipocalin protein family: structure and function. Biochem J. 318(Pt 1):1–14.

Forman-Rubinsky R, Cohen JD, Sundaram MV. 2017. Lipocalins are required for apical extracellular matrix organization and remodeling in *Caenorhabditis elegans*. Genetics. 207:625–642.

Gill HK, Cohen JD, Ayala-Figueroa J, Forman-Rubinsky R, Poggioli C, *et al.* 2016. Integrity of narrow epithelial tubes in the *C. elegans* excretory system requires a transient luminal matrix. PLoS Genet. 12:e1006205.

Greenwald IS, Sternberg PW, Horvitz HR. 1983. The *lin*-12 locus specifies cell fates in *Caenorhabditis elegans*. Cell. 34:435–444.

Hall ET, Cleverdon ER, Ogden SK. 2019. Dispatching sonic Hedgehog: molecular mechanisms controlling deployment. Trends Cell Biol. 29:385–395.

Hao L, Aspöck G, Bürglin TR. 2006a. The Hedgehog-related gene *wrt*-5 is essential for hypodermal development in *Caenorhabditis elegans*. Dev Biol. 290:323–336.

Hao L, Johnsen R, Lauter G, Baillie D, Bürglin TR. 2006b. Comprehensive analysis of gene expression patterns of Hedgehog-related genes. BMC Genomics. 7:280.

Heiman MG, Shaham S. 2009. DEX-1 and DYF-7 establish sensory dendrite length by anchoring dendritic tips during cell migration. Cell. 137:344–355.

Hendriks GJ, Gaidatzis D, Aeschimann F, Großhans H. 2014. Extensive oscillatory gene expression during *C. elegans* larval development. Mol Cell. 53:380–392.

Hishida R, Ishihara T, Kondo K, Katsura I. 1996. *hch*-1, a gene required for normal hatching and normal migration of a neuroblast in *C. elegans*, encodes a protein related to TOLLOID and BMP-1. EMBO J. 15:4111–4122.

Hofmann K, Stoffel W. 1993. TMbase—a database of membrane spanning protein segments. Biol Chem Hoppe Seyler. 347: 166–171.

Hu A, Song BL. 2019. The interplay of patched, smoothened and cholesterol in Hedgehog signaling. Curr Opin Cell Biol. 61: 31–38.

Kamath RS, Ahringer J. 2003. Genome-wide RNAi screening in *Caenorhabditis elegans*. Methods. 30:313–321.

Katz SS, Maybrun C, Maul-Newby HM, Frand AR. 2018. Non-canonical apical constriction shapes emergent matrices in *C. elegans*. bioRxiv. doi:10.1101/189951.

Kelley M, Yochem J, Krieg M, Calixto A, Heiman MG, *et al.* 2015. FBN-1, a fibrillin-related protein, is required for resistance of the epidermis to mechanical deformation during *C. elegans* embryogenesis. eLife. 4:e06565.

Kolotuev I, Apaydin A, Labouesse M. 2009. Secretion of Hedgehog-related peptides and WNT during *Caenorhabditis elegans* development. Traffic. 10:803–810.

Konířová J, Oltová J, Corlett A, Kopycińska J, Kolář M, *et al.* 2017. Modulated DISP3/PTCHD2 expression influences neural stem cell fate decisions. Sci Rep. 7:41597.

Kuwabara PE, Labouesse M. 2002. The sterol-sensing domain: multiple families, a unique role? Trends Genet. 18:193–201.

Liégeois S, Benedetto A, Garnier JM, Schwab Y, Labouesse M. 2006. The V0-ATPase mediates apical secretion of exosomes containing Hedgehog-related proteins in *Caenorhabditis elegans*. J Cell Biol. 173:949–961.

Low IIC, Williams CR, Chong MK, McLachlan IG, Wierbowski BM, *et al.* 2019. Morphogenesis of neurons and glia within an epithelium. Development. 146:dev171124.

Mancuso VP, Parry JM, Storer L, Poggioli C, Nguyen KC, *et al.* 2012. Extracellular leucine-rich repeat proteins are required to organize the apical extracellular matrix and maintain epithelial junction integrity in *C. elegans*. Development. 139:979–990.

McMahon L, Muriel JM, Roberts B, Quinn M, Johnstone IL. 2003. Two sets of interacting collagens form functionally distinct substructures within a *Caenorhabditis elegans* extracellular matrix. Mol Biol Cell. 14:1366–1378.

Melly G, Purdy GE. 2019. MmpL proteins in physiology and pathogenesis of *M. tuberculosis*. Microorganisms. 7: 70.

Miao R, Li M, Zhang Q, Yang C, Wang X. 2020. An ECM-to-Nucleus signaling pathway activates lysosomes for *C. elegans* larval development. Dev Cell. 52:21–37.e25.

Michaux G, Gansmuller A, Hindelang C, Labouesse M. 2000. CHE-14, a protein with a sterol-sensing domain, is required for apical sorting in *C. elegans* ectodermal epithelial cells. Curr Biol. 10: 1098–1107.

Moerman DG, Barstead RJ. 2008. Towards a mutation in every gene in *Caenorhabditis elegans*. Brief Funct Genomic Proteomic. 7:195–204.

Moribe H, Yochem J, Yamada H, Tabuse Y, Fujimoto T, *et al.* 2004. Tetraspanin protein (TSP-15) is required for epidermal integrity in *Caenorhabditis elegans*. J Cell Sci. 117:5209–5220.

Nikaido H. 2018. RND transporters in the living world. Res Microbiol. 169:363–371.

Oikonomou G, Perens EA, Lu Y, Watanabe S, Jorgensen EM, *et al.* 2011. Opposing activities of LIT-1/NLK and DAF-6/patched-related direct sensory compartment morphogenesis in *C. elegans*. PLoS Biol. 9:e1001121.

Olson SK, Greenan G, Desai A, Muller-Reichert T, Oegema K. 2012. Hierarchical assembly of the eggshell and permeability barrier in *C. elegans*. J Cell Biol. 198:731–748.

Packer JS, Zhu Q, Huynh C, Sivaramakrishnan P, Preston E, *et al.* 2019. A lineage-resolved molecular atlas of *C. elegans* embryogenesis at single-cell resolution. Science. 365:eaax1971.

Page AP, Johnstone IL. 2007. The cuticle.(March 19, 2007), *WormBook*, ed. The *C. elegans* Research Community, WormBook, doi/10.1895/wormbook.1.138.1, http://www.wormbook.org.

Pedelacq JD, Cabantous S, Tran T, Terwilliger TC, Waldo GS. 2006. Engineering and characterization of a superfolder green fluorescent protein. Nat Biotechnol. 24:79–88.

Perens EA, Shaham S. 2005. *C. elegans daf-6* encodes a patched-related protein required for lumen formation. Dev Cell. 8:893–906.

Petrov K, Wierbowski BM, Liu J, Salic A. 2020. Distinct cation gradients power cholesterol transport at different key points in the Hedgehog signaling pathway. Dev Cell. 55:314–327.e7.

Pfeffer SR. 2019. NPC intracellular cholesterol transporter 1 (NPC1)-mediated cholesterol export from lysosomes. J Biol Chem. 294:1706–1709.

Priess JR, Hirsh DI. 1986. *Caenorhabditis elegans* morphogenesis: the role of the cytoskeleton in elongation of the embryo. Dev Biol. 117:156–173.

Pu P, Stone CE, Burdick JT, Murray JI, Sundaram MV. 2017. The lipocalin LPR-1 cooperates with LIN-3/EGF signaling to maintain narrow tube integrity in *Caenorhabditis elegans*. Genetics. 205:1247–1260.

Sandhu A, Badal D, Sheokand R, Tyagi S, Singh V. 2021. Specific collagens maintain the cuticle permeability barrier in *Caenorhabditis elegans*. Genetics. 217(3):iyaa047.

Schultz RD, Gumienny TL. 2012. Visualization of *Caenorhabditis elegans* cuticular structures using the lipophilic vital dye DiI. J Vis Exp. 59:e3362.

Schwartz ML, Jorgensen EM. 2016. SapTrap, a toolkit for high-throughput CRISPR/Cas9 gene modification in *Caenorhabditis elegans*. Genetics. 202:1277–1288.

Stein KK, Golden A. 2018. The *C. elegans* eggshell. WormBook. 2018: 1–36.

Steinhoff JS, Lass A, Schupp M. 2021. Biological functions of RBP4 and its relevance for human diseases. Front Physiol. 12:659977.

Stone CE, Hall DH, Sundaram MV. 2009. Lipocalin signaling controls unicellular tube development in the *Caenorhabditis elegans* excretory system. Dev Biol. 329:201–211.

Templeman NM, Cota V, Keyes W, Kaletsky R, Murphy CT. 2020. CREB non-autonomously controls reproductive aging through Hedgehog/patched signaling. Dev Cell. 54:92–105.e5.

Thein MC, McCormack G, Winter AD, Johnstone IL, Shoemaker CB, *et al.* 2003. *Caenorhabditis elegans* exoskeleton collagen COL-19: an adult-specific marker for collagen modification and assembly, and the analysis of organismal morphology. Dev Dyn. 226: 523–539.

Timmons L, Court DL, Fire A. 2001. Ingestion of bacterially expressed dsRNAs can produce specific and potent genetic interference in Caenorhabditis elegans. Gene. 263:103–112.

Torrico B, Fernàndez-Castillo N, Hervás A, Milà M, Salgado M, *et al.* 2015. Contribution of common and rare variants of the PTCHD1 gene to autism spectrum disorders and intellectual disability. Eur J Hum Genet. 23:1694–1701.

Ung DC, Iacono G, Méziane H, Blanchard E, Papon MA, *et al.* 2018. Ptchd1 deficiency induces excitatory synaptic and cognitive dysfunctions in mouse. Mol Psychiatry. 23:1356–1367.

Vuong-Brender TTK, Suman SK, Labouesse M. 2017. The apical ECM preserves embryonic integrity and distributes mechanical stress during morphogenesis. Development. 144:4336–4349.

Zhang Y, Bulkley DP, Xin Y, Roberts KJ, Asarnow DE, *et al.* 2018. Structural basis for cholesterol transport-like activity of the Hedgehog receptor patched. Cell. 175:1352–1364.e14.

Zhong Y, Gu LJ, Sun XG, Yang SH, Zhang XH. 2014. Comprehensive analysis of patched domain-containing genes reveals a unique evolutionary pattern. Genet Mol Res. 13:7318–7331.

Zikova M, Corlett A, Bendova Z, Pajer P, Bartunek P. 2009. DISP3, a sterol-sensing domain-containing protein that links thyroid hormone action and cholesterol metabolism. Mol Endocrinol. 23: 520–528.

Zugasti O, Rajan J, Kuwabara PE. 2005. The function and expansion of the Patched- and Hedgehog-related homologs in *C. elegans*. Genome Res. 15:1402–1410.

Communicating editor: V. Reinke